IEEE Access
Multidisciplinary ⋮ Rapid Review ⋮ Open Access Journal

Received January 11, 2021, accepted February 8, 2021, date of publication February 19, 2021, date of current version March 2, 2021.

Digital Object Identifier 10.1109/ACCESS.2021.3060436

Robust Scalar Control of Synchronous Reluctance Motor With Optimal Efficiency by MTPA Control

LON-JAY CHENG AND MI-CHING TSAI, (Fellow, IEEE)
Department of Mechanical Engineering, National Cheng Kung University, Tainan 70101, Taiwan
Corresponding author: Mi-Ching Tsai (mctsai@mail.ncku.edu.tw)

This work was supported by the Ministry of Science and Technology (MOST), Taiwan, under Grant MOST 109-2622-8-006-005.

ABSTRACT In order to achieve improved performance and efficiency of domestic and industrial fan/pump applications using low-cost solutions, the synchronous reluctance motors (SynRMs) remains a better choice than induction motors (IMs) which are still widely used for such applications despite its low efficiency during low speed operation. However, due to the lack of self-start capability the SynRMs need external drive and speed control algorithm to properly operate, which increases the production cost. For the purpose of providing low cost solutions for the SynRMs speed control, this paper presents a stable, reliable and robust scalar control for SynRMs. This control strategy implements the maximum torque per ampere loop for high efficiency operation and online parameter estimation for robust performance. The proposed solution presented in this paper can be implemented using a low cost MCU in PWM inverter with lower carrier frequency, thereby making the low cost SynRM drive for fan/pump application feasible and practical.

INDEX TERMS Synchronous reluctance motor, scalar control, SynRM, MTPA, V/F control, online inductance estimation.

I. INTRODUCTION

The induction motors (IMs), which are widely used for most electric powered machines, such as fans, pumps, compressors, and other industrial and domestic applications, are still the main choice of drive technology. In the search to reduce energy consumption and lower the environmental impact, the attainment of higher efficiency levels poses a major challenge for IMs applications. To increase efficiency, other alternatives would be permanent magnetic motors or synchronous reluctance motors [1]. Although the permanent magnetic synchronous motors (PMSMs) have the highest efficiency, it is highly dependent on rare-earth magnets. Another choice is the synchronous reluctance motor (SynRM), which requires no magnets, has a simple structure, and can be implemented using highly dynamic control, which means SynRMs require highly precise tuning of the inverter to work properly, and thus, have higher cost than the IMs solution. Even though the manufacturing cost of SynRMs is higher than that of IMs, if various conditions, such as the control method [2] [3], inverter cost, etc., are considered, SynRMs would be a decent and low-cost solution to replace IMs.

The associate editor coordinating the review of this manuscript and approving it for publication was Javed Iqbal.

The torque of SynRMs are generated by reluctance power, which means that the machine is neither fitted with permanent magnets, nor are there electrical windings in the rotor, as the rotor is made of highly permeable soft magnetic electric laminations. The major losses occur in the stator, which could be easily cooled from outside the motor [4]. As a result, suitably constructed SynRMs are tolerant to overloading, which makes them ideal for operation in rugged environments. Reluctance motors and inverters are specifically designed to work together to create an integrated drive system for fan/pump applications, and they can operate more efficiently in comparison to induction motors.

SynRMs can offer better energy efficiency for lower output applications than IM, particularly in the low power range, the partial load range, and at the rated operating point. In addition to high efficiency, SynRMs also have high performance density. In order to leverage the maximum energy-saving potential, a robust and simple control algorithm is required for motor drives equipped with SynRMs.

Among the control methods for SynRMs, the field-oriented control (FOC) vector control [5], [6] is widely used for most industrial applications. As shown in Figure 1, FOC requires a position/speed observer to exert coordinate transformation to achieve dq-axis current control, and all of the controllers or

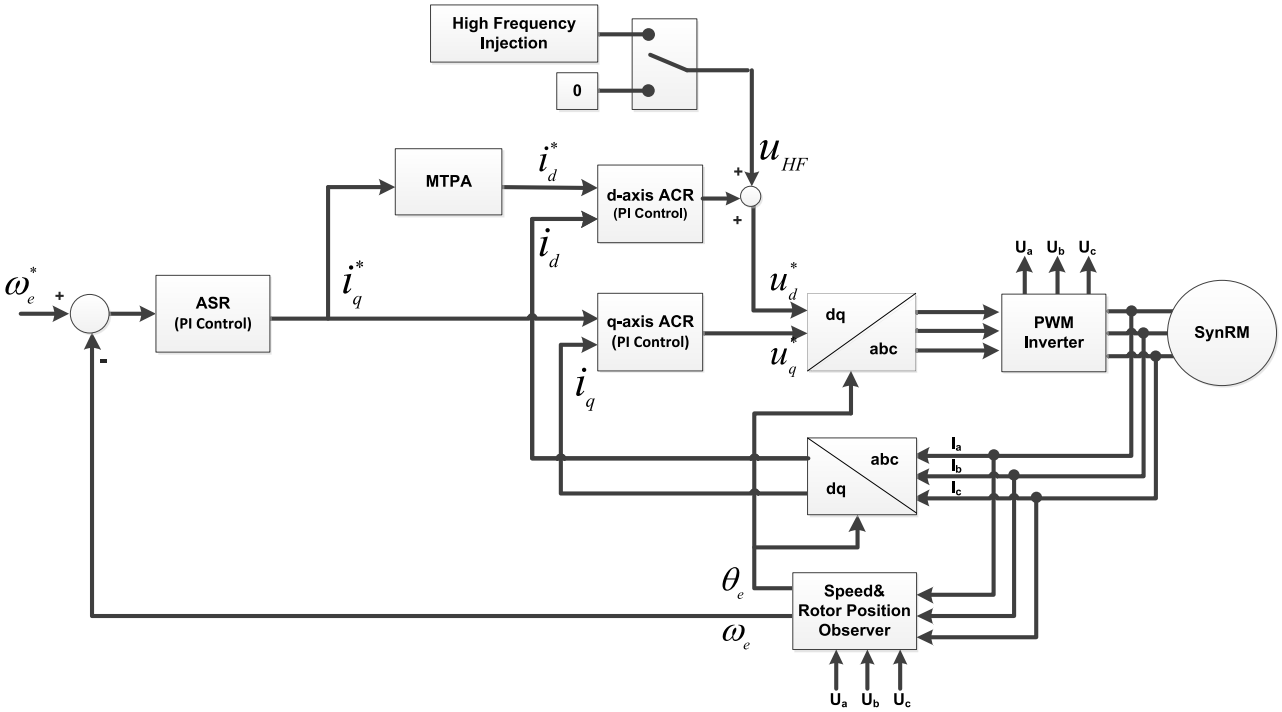

FIGURE 1. Block Diagram of FOC Control for SynRM.

observers require an accurate motor model to achieve decent speed and torque control. FOC control requires high MCU performance and high precision current sensor for high performance current vector and position estimation, thus increasing the cost of drives for electronic devices. Furthermore, FOC control requires a higher carrier ratio than scalar control, meaning FOC control needs a higher switch frequency for IGBT, which increases the cost of IGBT and cooling components.

In order to reduce the drive costs for SynRM, a robust scalar control [7] is proposed, as shown in Figure 2. As the scalar control needs no current control or speed/position observer, it means a low cost MCU and current sensor could be used to achieve decent control performance. Moreover, the low switching frequency of the IGBT component means inverters can be made by the low-cost power stage and cooling components due to lower switching loss. The two important issues of SynRM scalar control are stability control and efficiency optimization. In order to make scalar control stable for speed control in SynRMs, a stabilized loop is presented in [7], [8]. Regarding efficiency optimization, various kinds of voltage compensation strategies were proposed by [9]–[12]. As presented in [9], the power factor is used to compensate the voltage when load disturbance is exerted on the SynRM. While voltage compensation through a power factor features fast response to load disturbance, it is difficult to design its control gain. Another type of compensation strategy uses reactive power to adjust the voltage as the load disturbance changes. The reactive power reference is calculated by the load level and optimized by the maximum torque per ampere (MTPA) rule of SynRM [10].

When the output voltage is well compensated by means of the reactive power method, efficiency and optimized reactive power control are optimized; however, reactive power calculation is highly dependent on precise motor inductance, which varies with respect to load current [3]. Thus, in order to address precise reactive power calculation, scalar control with an online inductance estimation is proposed in this paper to achieve robust control performance with dynamic load disturbance according to literatures [13]–[19].

To show how the robust scalar control of SynRM is designed, section II illustrates the basic control framework of scalar control for SynRMs, which consists of a stabilization loop through frequency compensation, and an efficiency optimization loop through voltage compensation. Section III depicts an online motor parameter estimation for SynRM, with which the reactive power can be precisely calculated. Section IV shows the simulation result of the proposed scalar control, and Section V shows the experiment results. Finally, the conclusions are given at the end of this paper.

II. SCALAR CONTROL OF SYNCHRONOUS MOTOR CONTROL METHODOLOGY

To derive a related control algorithm, the SynRM electric model is shown in Equation (1) and the mechanical model is shown in Equation (2). The equivalent circuit of the dq-axis electric model is shown in Figure 3, which features a RL-circuit. The symbols used in the motor model equations are defined in Table 1. Coordinate definitions of dq-axis are

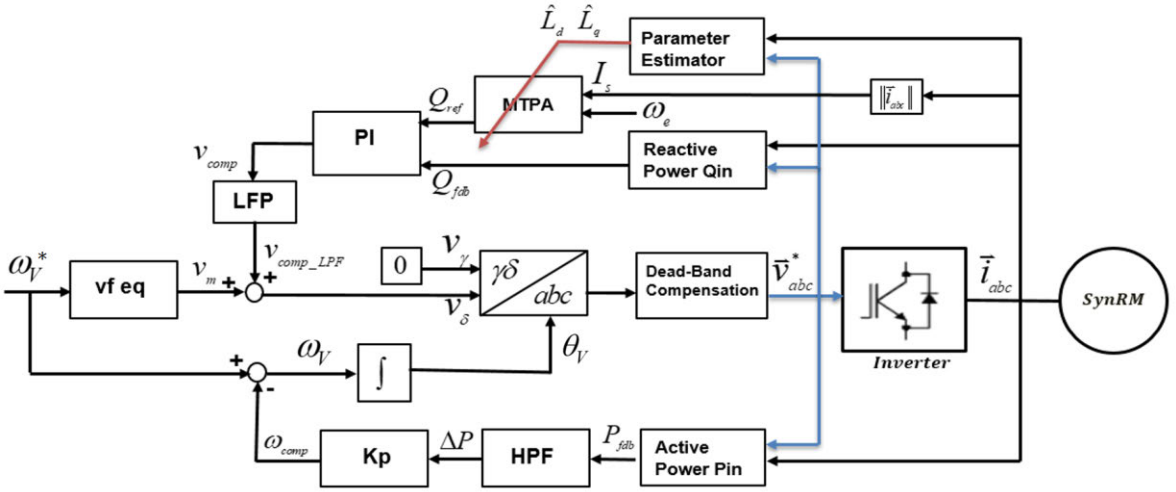

FIGURE 2. Block Diagram of Scalar Control for SynRM.

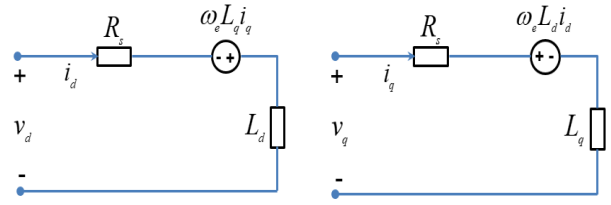

(a) Equivalent circuit of d-axis (b) Equivalent circuit of q-axis

FIGURE 3. Equivalent circuit of SynRM.

shown in Figure 4 and Figure 5.

$$\begin{aligned} pi_d &= -\frac{R_s}{L_d} i_d + \omega_e \frac{L_q}{L_d} i_q + \frac{v_d}{L_d} \\ pi_q &= -\omega_e \frac{L_d}{L_q} i_d - \frac{R_s}{L_q} i_q + \frac{v_q}{L_q} \end{aligned} \tag{1}$$

$$\begin{aligned} p\omega_e &= \frac{P_n}{2}\frac{T_e}{J} - \frac{B}{J}\omega_e - \frac{P_n}{2}\frac{T_L}{J} \\ p\varphi &= \omega_V - \omega_e \end{aligned} \tag{2}$$

A. STEADY STATE MODEL OF SYNRM

When a SynRM operates in the steady state, the output voltage vector can be expressed as Equation (3). According to the vector diagram in Figure 5, the amplitude of output voltage vector $\vec{V}_s$ can be calculated by the steady state current I_s and power factor $\cos\phi$, which can be easily obtained by the reactive and active power calculations of Equation (4).

$$\vec{V}_s = \begin{bmatrix} V_d \\ V_q \end{bmatrix} = \begin{bmatrix} R_s I_d - \omega_e L_q I_q \\ R_s I_q + \omega_e L_d I_d \end{bmatrix} \tag{3}$$

$$\begin{aligned} \left|\vec{V}_s\right| &= R_s \left|\vec{I}_s\right| \cos\phi \\ &+ \sqrt{(\omega_e L_d I_d)^2 + (\omega_e L_q I_q)^2 - (R_s I_s \sin\phi)^2} \end{aligned} \tag{4}$$

B. STABILITY ANALYSIS OF SCALAR CONTROL

Regarding the stability analysis, the small signal model [7] is described by Equation (5) which is derived from

TABLE 1. The definitions of the parameters.

Definition	Symbol
Motor inertia	J
Damping Factor	B
Voltage Angle	θ_V
Rotor Electrical Angle	θ_e
Electric Torque	T_e
Load Torque	T_L
Voltage Frequency	$\omega_V = 2\pi f_V = \dot{\theta}_V$
Rotor Electrical Frequency	$\omega_e = 2\pi f_e = \dot{\theta}_e$
dq-axis Inductance	L_d 、 L_q
Motor Poles	P_n
differential operator d/dt	p
Load angle	φ
dq-axis Current	i_d i_q
γδ-axis Current	i_γ i_δ
dq-axis Voltage	v_d v_q
γδ-axis Voltage	v_γ v_δ
Steady state voltage vector	$\vec{V}_s = \begin{bmatrix} V_d & V_q \end{bmatrix}^T$
Steady state current vector	$\vec{I}_s = \begin{bmatrix} I_d & I_q \end{bmatrix}^T$
power factor	$\cos\phi = \frac{P_{fdb}}{\sqrt{P_{fdb}^2 + Q_{fdb}^2}}$
Real Power	$P_{fdb} = i_\gamma v_\gamma + i_\delta v_\delta$
Reactive Power	$Q_{fdb} = i_\gamma v_\delta - i_\delta v_\gamma$

partial derivation of Equations (1) and (2) at a specified steady state, $X_0 = \begin{bmatrix} I_{d0} & I_{q0} & \omega_{e0} & \varphi_0 \end{bmatrix}^T$, of state $x = \begin{bmatrix} i_d & i_q & \omega_e & \varphi \end{bmatrix}^T$. Regarding the SynRM with parameters, as listed in Table 2 of Section IV, the root locus of Equation (5) for various stator frequency f_e is shown in Figure 6(a) under a specified condition, namely,

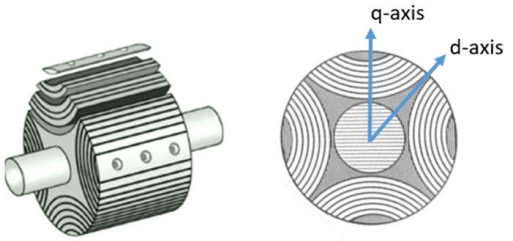

FIGURE 4. Coordinate definition of SynRM.

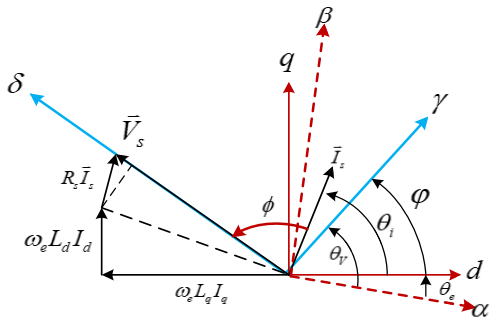

FIGURE 5. Steady state voltage and current vector diagram.

$X_0 = \begin{bmatrix} 3.9 & 3.9 & 2\pi f_e & 0 \end{bmatrix}^T$, $\phi = 0$ and V_s is calculated by Equation (4). The root locus for the various f_e reveals that unstable poles would appear when the frequency is sufficiently high, as shown in Figure 6(b).

$$p\begin{bmatrix} \Delta i_d \\ \Delta i_q \\ \Delta\omega_e \\ \Delta\varphi \end{bmatrix} = \begin{bmatrix} -\frac{R_s}{L_d} & \frac{L_q}{L_d}\omega_{e0} & \frac{L_q}{L_d}I_{q0} & -\frac{V_s\cos\varphi_0}{L_d} \\ -\frac{L_d}{L_q}\omega_{e0} & -\frac{R_s}{L_q} & -\frac{L_d}{L_q}I_{d0} & -\frac{V_s\sin\varphi_0}{L_q} \\ K_J I_{d0} & K_J I_{q0} & -\frac{B}{J} & 0 \\ 0 & 0 & -1 & 0 \end{bmatrix} \times \begin{bmatrix} \Delta i_d \\ \Delta i_q \\ \Delta\omega_e \\ \Delta\varphi \end{bmatrix} + \begin{bmatrix} 0 \\ 0 \\ -\frac{P_n}{2J} \\ 0 \end{bmatrix} \Delta T_L \quad (5)$$

where

$$\Delta x = \begin{bmatrix} \Delta i_d & \Delta i_q & \Delta\omega_e & \Delta\varphi \end{bmatrix}^T = x - X_0 = \begin{bmatrix} i_d & i_q & \omega_e & \varphi \end{bmatrix}^T - \begin{bmatrix} I_{d0} & I_{q0} & \omega_{e0} & \varphi_0 \end{bmatrix}^T$$

$$K_J = \frac{3}{2J}\left(\frac{P_n}{2}\right)^2 (L_d - L_q)$$

To improve the above-described instability, previous literature, such as [7], proposed a stabilized loop by frequency compensation, as shown in Figure 2 and Figure 7. A high pass filter (HPF) is used to filter out the power disturbance, which reflects the speed vibration caused by the load torque.

Once the load disturbance is filtered out by the HPF, a feedback loop can be added into the scalar control loop, and the overall small signal model can be expressed as Equation (6). If a proper K_p gain is given, as shown in Figure 7, the root locus of the compensated system reveals

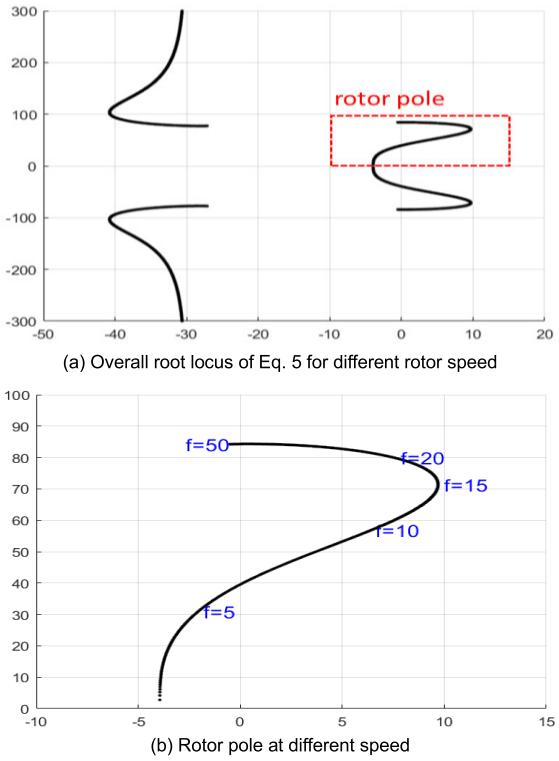

(a) Overall root locus of Eq. 5 for different rotor speed

(b) Rotor pole at different speed

FIGURE 6. Root locus of Eq. 5 for different rotor speed.

that the system is stable for all operating speeds, as shown in Figure 9(a) near the steady state, in which $X_0 = \begin{bmatrix} 3.9 & 3.9 & 2\pi f_e & 0 & 2\pi f_V \end{bmatrix}^T$; $\phi = 0$, and V_s is calculated by Equation (4).

$$p\begin{bmatrix} \Delta i_d \\ \Delta i_q \\ \Delta\omega_e \\ \Delta\varphi \\ \Delta\omega_V \end{bmatrix} = \begin{bmatrix} -\frac{R_s}{L_d} & \frac{L_q}{L_d}\omega_{e0} & \frac{L_q}{L_d}I_{q0} & -\frac{V_s\cos\varphi_0}{L_d} & 0 \\ -\frac{L_d}{L_q}\omega_{e0} & -\frac{R_s}{L_q} & -\frac{L_d}{L_q}I_{d0} & -\frac{V_s\sin\varphi_0}{L_q} & 0 \\ K_J I_{d0} & K_J I_{q0} & -\frac{B}{J} & 0 & 0 \\ 0 & 0 & -1 & 0 & 1 \\ A_{51} & A_{52} & A_{53} & A_{54} & A_{55} \end{bmatrix} \times \begin{bmatrix} \Delta i_d \\ \Delta i_q \\ \Delta\omega_e \\ \Delta\varphi \\ \Delta\omega_V \end{bmatrix} + \begin{bmatrix} 0 \\ 0 \\ -\frac{P_n}{2J} \\ 0 \\ 0 \end{bmatrix} \Delta T_L \quad (6)$$

where

$$\Delta x = \begin{bmatrix} \Delta i_d & \Delta i_q & \Delta\omega_e & \Delta\varphi & \Delta\omega_V \end{bmatrix}^T = x - X_0 = \begin{bmatrix} i_d & i_q & \omega_e & \varphi & \omega_V \end{bmatrix}^T - \begin{bmatrix} I_{d0} & I_{q0} & \omega_{e0} & \varphi_0 & \omega_{V0} \end{bmatrix}^T$$

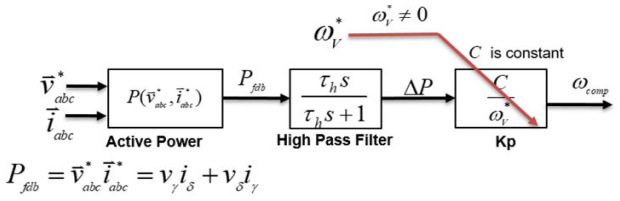

FIGURE 7. Block diagram of the stabilized loop[7].

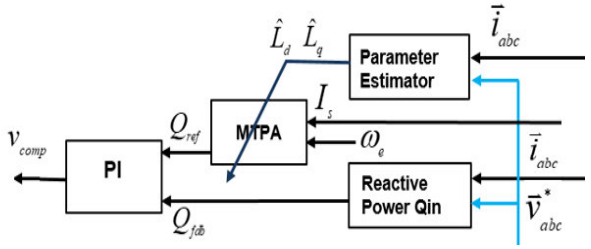

FIGURE 8. Block diagram of the efficiency optimized loop.

$$K_c = \frac{3}{2}K_p V_s;\ K_P = C/\omega_V^*;\ \sigma = \frac{L_q}{L_d};\ \tau_s = \frac{L_d}{R_s};$$

$$\mathrm{A}_{51} = K_c(\omega_{V0}\frac{\cos\varphi_0}{\sigma} - \frac{\sin\varphi_0}{\tau_s});$$

$$\mathrm{A}_{52} = K_c(\frac{\cos\varphi_0}{\sigma\tau_s} + \omega_{V0}\sigma\sin\varphi)$$

$$\mathrm{A}_{53} = K_c\left[(\sigma-1)I_{q0}\sin\varphi_0 + \frac{1-\sigma}{\sigma}I_{d0}\cos\varphi_0\right]$$

$$\mathrm{A}_{54} = K_c\left[(\omega_{V0}\sigma I_{q0} - \frac{I_{d0}}{\tau_s})\cos\varphi_0 - \frac{V_s(\sigma-1)\sin(2\varphi_0)}{\sigma L_d} - (\frac{\omega_{V0}I_{d0}}{\sigma} + \frac{I_{q0}}{\sigma\tau_s})\sin\varphi_0\right]$$

$$\mathrm{A}_{55} = K_c(I_{q0}\sin\varphi_0 + I_{d0}\cos\varphi_0) - \frac{1}{\tau_h}$$

Although a frequency compensation loop can stabilize the SynRM scalar control, even with a frequency stabilized loop, unstable poles would still appear if an improper voltage command is given to the system, as shown in Figure 9(b); for example $X_0 = \begin{bmatrix} 3.9 & 3.9 & 2\pi f_e & 0 & 2\pi f_V \end{bmatrix}$, $\phi = 0$ and $V_s = 125\%$ of Equation (4).

Summarily, both the stabilization loop and a proper voltage command should work together to stabilize the SynRM scalar control. The proper voltage command is calculated according to Equation (4), and should also be regulated by a MTPA efficiency-optimized loop, which is described in detail in subsection II.C.

C. EFFICIENCY OPTIMIZATION OF SCALAR CONTROL

As mentioned in subsection II.B, the voltage command given by Equation (4) must be compensated by some kind of algorithm if scalar control is expected to achieve a certain performance index, such as the maximum efficiency or the optimum power factor. For example, the voltage command is regulated to achieve the optimal power factor [9] or to obtain the maximum torque per amp (MTPA) [10]–[12].

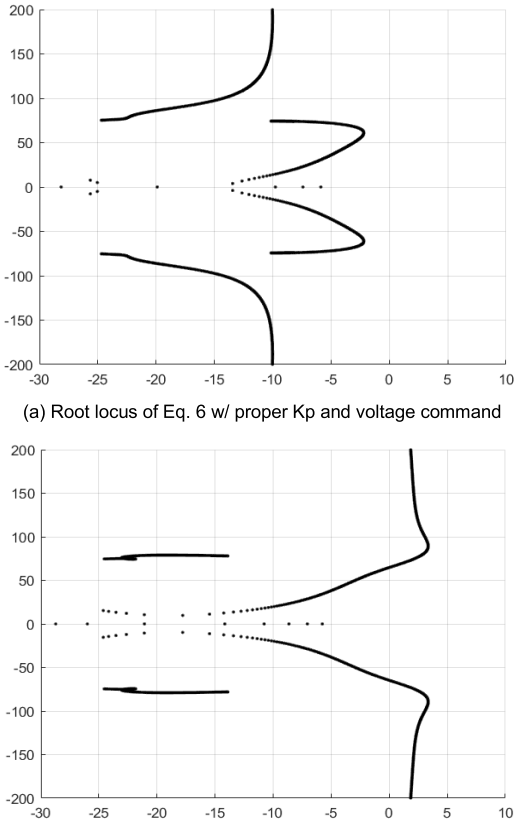

(a) Root locus of Eq. 6 w/ proper Kp and voltage command

(b) Root locus of Eq. 6 w/ proper K_p and improper voltage command

FIGURE 9. Root locus of Equation 6 with respect to rotor speed and different voltage command.

Some of these algorithms use reactive power to adjust voltage and increase efficiency. As shown in Figure 8, the reactive power Q_{ref}, as expressed in Equation (7), can be calculated by i_d and i_q, and then, Q_{ref} is set as the reference value of the PI controller. However, in scalar control, rotor position θ_e is unknown, which means the dq-axis currents i_d and i_q are not available to calculate the reactive power. Therefore, an equation that does not contain i_d and i_q, is required for the calculation of reactive power reference in scalar control.

As shown in [5], if current angle θ_i equals 45^o, meaning $i_d = i_q = \sqrt{2}/2\mathrm{i}_s$, then SynRM can operate in the MTPA condition, thus, in MTPA operation, i_d and i_q can be replaced by $\sqrt{2}i_s/2$. Then reactive power reference Q_{ref} can also be expressed as a function of i_s only, as derived in Equation (7). Therefore, once i_s is calculated from $i_s = \sqrt{i_\gamma^2 + i_\delta^2}$, Q_{ref} can be calculated merely by i_s, and the position estimator is not necessary, which reduces the complexity of the control structure.

$$\begin{aligned} Q_{ref} &= \frac{3}{2}\omega_e(L_d i_d^2 + L_q i_q^2) \\ &= \frac{3}{2}\omega_e(L_d\frac{1}{2}i_s^2 + L_q\frac{1}{2}i_s^2) = \frac{3}{4}\omega_e i_s^2(L_d + L_q) \end{aligned} \quad (7)$$

However, Q_{ref} for the MTPA condition in Equation (7) is a function of the stator current and motor inductance, which varies with the output current level [3]. When the

output current increases with respect to the loading torque, the inductance would decrease as well. If Q_{ref} is calculated by constant L_d, it will become higher than that calculated by the actual L_d, which means that the PI controller will generate a higher voltage command than the ideal controller due to the use of an improperly high Q_{ref}, as calculated by constant L_d. If an improperly high voltage is given to the scalar control of SynRM, unstable poles would appear, as shown in Figure 9(b). Therefore, to achieve robust control performance, the inductance L_d should be estimated online for the precise calculation of Q_{ref} and proper compensation voltage of MTPA.

III. ONLINE INDUCTANCE ESTIMATION FOR ROBUST SCALAR CONTROL

In order to further improve the performance of the MTPA voltage compensation loop, an online estimation of L_d inductance is very critical to calculate accurate reactive power in Figure 8. For the inductance estimation, some literatures including [13], [15]–[17] have made significant contributions to parameter estimation technique; however, when it comes to scalar control, there is more room for improvement which anchors on the shortcoming of previous researches. [13], [17] needed motor positioning to get accurate estimation but scalar control has no rotor position to control this algorithm. [15], [18] used recursive least square (RLS) method which is sensitive to speed accuracy and cannot make accurate estimations under light/no load condition. Due to the matrix operation involved in [16]'s method, higher CPU resources are required compared to other approaches. In order to provide reliable and accurate parameters for scalar control, this paper proposed a modified online parameter estimation in $\gamma\delta$-axis with details of the estimation rules. The proposed approach employs online estimation approach, and its needed algorithm requires fewer computational resources compared to other methods. Details of the proposed method are derived as following steps. The voltage model of SynRMs can be expressed as Equation (8) and can be rearranged as Equation (9).

$$\begin{bmatrix} u_d \\ u_q \end{bmatrix} = \begin{bmatrix} R_s & -\omega_e L_q \\ \omega_e L_d & R_s \end{bmatrix} \begin{bmatrix} i_d \\ i_q \end{bmatrix} + \begin{bmatrix} L_d & 0 \\ 0 & L_q \end{bmatrix} \begin{bmatrix} pi_d \\ pi_q \end{bmatrix} \tag{8}$$

$$\begin{bmatrix} u_d \\ u_q \end{bmatrix} = \begin{bmatrix} R_s & -\omega_e L_d \\ \omega_e L_d & R_s \end{bmatrix} \begin{bmatrix} i_d \\ i_q \end{bmatrix} + \begin{bmatrix} L_d & 0 \\ 0 & L_d \end{bmatrix} \begin{bmatrix} pi_d \\ pi_q \end{bmatrix} + \begin{bmatrix} \omega_e L_d i_q - \omega_e L_q i_q \\ pi_q L_q - pi_q L_d \end{bmatrix} \tag{9}$$

If λ_a, which is called extended flux, is substituted into Equation (9), a brief form of Equation (9) can be expressed as

$$\begin{bmatrix} u_d \\ u_q \end{bmatrix} = \begin{bmatrix} R_s & -\omega_e L_d \\ \omega_e L_d & R_s \end{bmatrix} \begin{bmatrix} i_d \\ i_q \end{bmatrix} + \begin{bmatrix} L_d & 0 \\ 0 & L_d \end{bmatrix} \begin{bmatrix} pi_d \\ pi_q \end{bmatrix} + \begin{bmatrix} \omega_e \lambda_a \\ -p\lambda_a \end{bmatrix}$$

where

$$\lambda_a = (L_d - L_q) i_q. \tag{10}$$

However, due to the lack of rotor position, Equation (10) must be transformed from the dq-axis to the alternative $\gamma\delta$-axis, as shown in Figure 5. After the coordinate transformation, the voltage model of SynRM in the $\gamma\delta$-axis can be expressed as

$$\begin{bmatrix} u_\gamma \\ u_\delta \end{bmatrix} = \begin{bmatrix} R_s & -\omega_e L_d \\ \omega_e L_d & R_s \end{bmatrix} \begin{bmatrix} i_\gamma \\ i_\delta \end{bmatrix} + \begin{bmatrix} L_d & 0 \\ 0 & L_d \end{bmatrix} \begin{bmatrix} pi_\gamma \\ pi_\delta \end{bmatrix} + \begin{bmatrix} \cos\varphi & -\sin\varphi \\ \sin\varphi & \cos\varphi \end{bmatrix} \begin{bmatrix} -\omega_e \lambda_a \\ p\lambda_a \end{bmatrix} \tag{11}$$

In order to obtain the observer dynamic equation, the current dynamic model is derived, as shown below

$$\begin{bmatrix} pi_\gamma \\ pi_\delta \end{bmatrix} = \begin{bmatrix} -\frac{R_s}{L_d} & \omega_e \\ -\omega_e & -\frac{R_s}{L_d} \end{bmatrix} \begin{bmatrix} i_\gamma \\ i_\delta \end{bmatrix} + \omega_e \left(\begin{bmatrix} \frac{\cos\varphi \lambda_a}{L_d} \\ \frac{\sin\varphi \lambda_a}{L_d} \end{bmatrix} + \begin{bmatrix} \frac{(p\lambda_a)\sin\varphi}{\omega_e L_d} \\ -\frac{(p\lambda_a)\cos\varphi}{\omega_e L_d} \end{bmatrix} \right) + \frac{1}{L_d} \begin{bmatrix} u_\gamma \\ u_\delta \end{bmatrix} \tag{12}$$

To further reduce the complexity of Equation (12), the extended flux is assumed to be constant during the parameter identification process, which means $p\lambda_a = 0$. A simplified current dynamic equation and observer model can be expressed as Equations (13) and (14), respectively.

$$\begin{bmatrix} pi_\gamma \\ pi_\delta \end{bmatrix} = \begin{bmatrix} -\frac{R_s}{L_d} & \omega_e \\ -\omega_e & -\frac{R_s}{L_d} \end{bmatrix} \begin{bmatrix} i_\gamma \\ i_\delta \end{bmatrix} + \omega_e \begin{bmatrix} \frac{\cos\varphi \lambda_a}{L_d} \\ \frac{\sin\varphi \lambda_a}{L_d} \end{bmatrix} + \frac{1}{L_d} \begin{bmatrix} u_\gamma \\ u_\delta \end{bmatrix} \tag{13}$$

$$\begin{bmatrix} p\hat{i}_\gamma \\ p\hat{i}_\delta \end{bmatrix} = \begin{bmatrix} -\frac{\hat{R}_s}{\hat{L}_d} & \omega_e \\ -\omega_e & -\frac{\hat{R}_s}{\hat{L}_d} \end{bmatrix} \begin{bmatrix} \hat{i}_\gamma \\ \hat{i}_\delta \end{bmatrix} + \omega_e \left(\begin{bmatrix} \frac{\cos\varphi \hat{\lambda}_a}{\hat{L}_d} \\ \frac{\sin\varphi \hat{\lambda}_a}{\hat{L}_d} \end{bmatrix} \right) + \frac{1}{\hat{L}_d} \begin{bmatrix} u_\gamma \\ u_\delta \end{bmatrix} \tag{14}$$

If Equation (14) is subtracted from Equation (13), the error dynamic model of the SynRM can be derived, as shown in Equation (15).

$$\begin{bmatrix} pe_\gamma \\ pe_\delta \end{bmatrix} = \begin{bmatrix} -\frac{R_s}{L_d} & \omega_e \\ -\omega_e & -\frac{R_s}{L_d} \end{bmatrix} \begin{bmatrix} e_\gamma \\ e_\delta \end{bmatrix} + \left(\frac{\hat{R}_s}{\hat{L}_d} - \frac{R_s}{L_d}\right) \begin{bmatrix} \hat{i}_\gamma \\ \hat{i}_\delta \end{bmatrix} + \left(\frac{\lambda_a}{L_d}\cos\varphi - \frac{\hat{\lambda}_a}{\hat{L}_d}\cos\varphi\right) \begin{bmatrix} \omega_e \\ 0 \end{bmatrix}$$

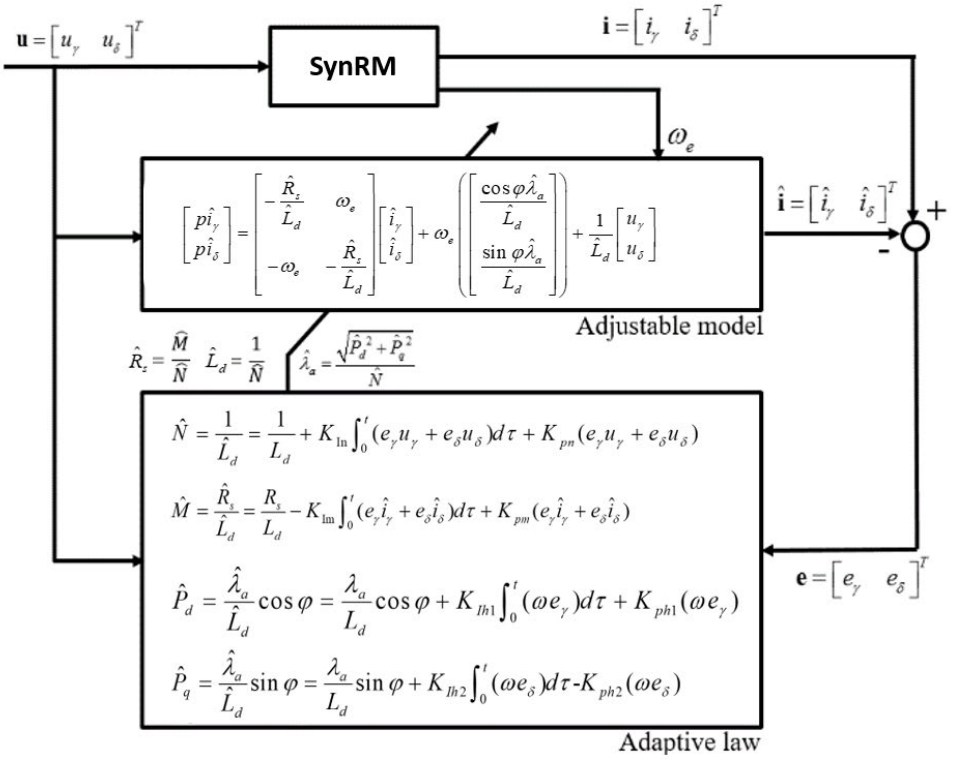

FIGURE 10. Block diagram of the SynRM parameters estimation.

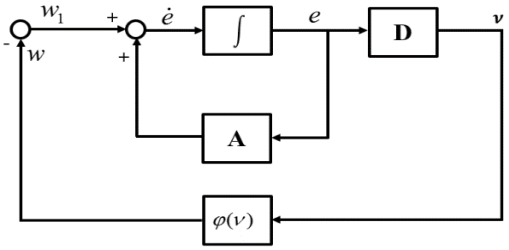

FIGURE 11. Equivalent block diagram of a linear system with nonlinear feedback.

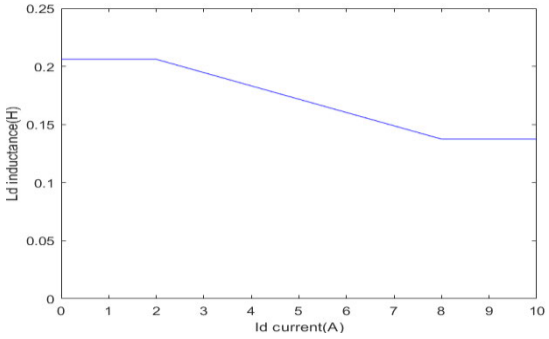

FIGURE 12. L_d-I_d curve of the simulation model.

$$+\left(\frac{\lambda_a}{L_d}\sin\varphi-\frac{\hat{\lambda}_a}{\hat{L}_d}\sin\varphi\right)\begin{bmatrix}0\\ \omega_e\end{bmatrix}+\left(\frac{1}{L_d}-\frac{1}{\hat{L}_d}\right)\begin{bmatrix}u_\gamma\\ u_\delta\end{bmatrix}$$

where

$$\begin{bmatrix}e_\gamma & e_\delta\end{bmatrix}^T=\begin{bmatrix}(i_\gamma-\hat{i}_\gamma) & (i_\delta-\hat{i}_\delta)\end{bmatrix}^T \tag{15}$$

Equation (15) can be further expressed as Equation (16), and the equivalent block diagram of this error equation can be expressed as Figure 11, which consists of a linear system ($p\vec{e}=\boldsymbol{A}\vec{e}$) and nonlinear feedback ($-\boldsymbol{I}_2\vec{w}$)

$$p\vec{e}=A\vec{e}+(-I\vec{w}) \quad \text{where} \quad \mathbf{A}=\begin{bmatrix}-\frac{R_s}{L_d} & \omega_e\\ -\omega_e & -\frac{R_s}{L_d}\end{bmatrix} \tag{16}$$

$$\vec{w}=\left(\frac{R_s}{L_d}-\frac{\hat{R}_s}{\hat{L}_d}\right)\begin{bmatrix}\hat{i}_\gamma\\ \hat{i}_\delta\end{bmatrix}+\left(\frac{1}{\hat{L}_d}-\frac{1}{L_d}\right)\begin{bmatrix}u_\gamma\\ u_\delta\end{bmatrix}$$

$$+\left(\frac{\hat{\lambda}_a}{\hat{L}_d}\cos\varphi-\frac{\lambda_a}{L_d}\cos\varphi\right)\begin{bmatrix}\omega_e\\ 0\end{bmatrix}$$
$$+\left(\frac{\hat{\lambda}_a}{\hat{L}_d}\sin\varphi-\frac{\lambda_a}{L_d}\sin\varphi\right)\begin{bmatrix}0\\ \omega_e\end{bmatrix}$$
$$=\vec{w}_1+\vec{w}_2+\vec{w}_3+\vec{w}_4 \tag{17}$$

According to Popov's hyper stability theory [13], if the system represented by Equation (16) satisfies the following two lemmas, the estimation system is stable and the estimation error eventually approaches zero.

Lemma (a): The equivalent transfer function of the linear term satisfies the definition of strictly positive real.

$$\boldsymbol{H}(s)=\boldsymbol{D}(s\boldsymbol{I}_2-\boldsymbol{A})^{-1} \tag{18}$$

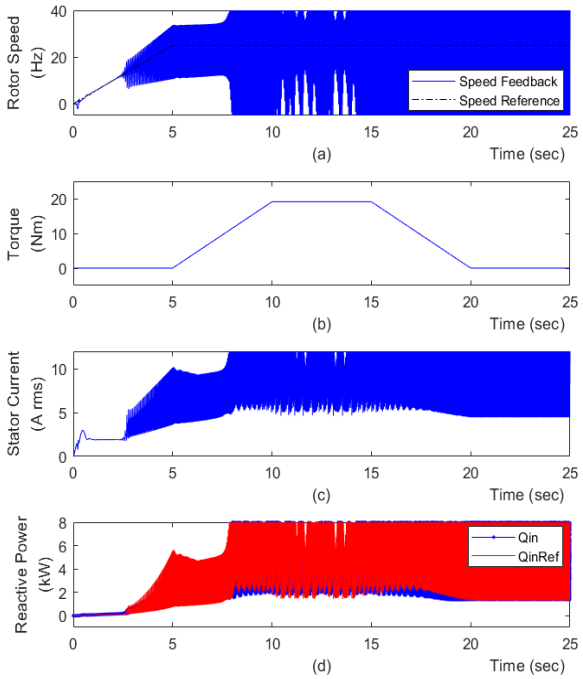

FIGURE 13. Ramp load test without stabilized loop. (a) Rotor speed; (b) Load torque=60% nominal torque (c) Stator current; (d) Reactive power.

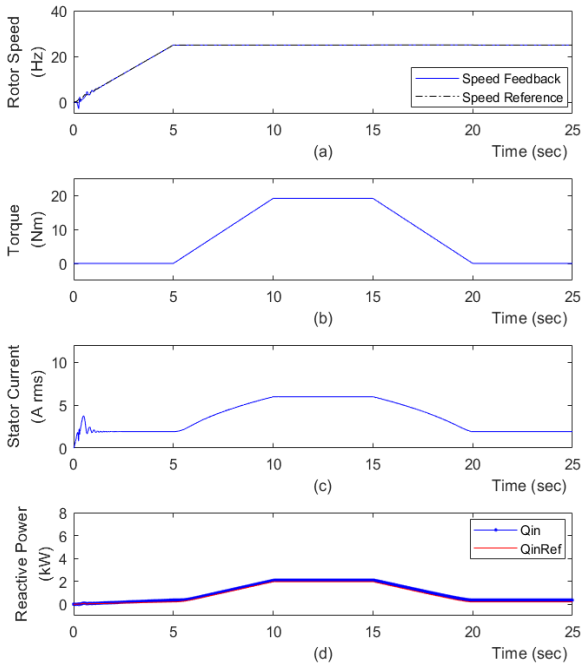

FIGURE 14. Ramp load test with stabilized loop. (a) Rotor speed; (b) Load torque=60% nominal torque (c) Stator current; (d) Reactive power.

Lemma (b): Nonlinear feedback term ($-\boldsymbol{I}_2\vec{w}$) must satisfy Popov's inequality, as shown in Equation (19).

$$\eta(0,t_0)=\int_0^{t_0}\vec{v}^T\vec{w}dt\geq-\kappa^2 \tag{19}$$

In order to simplify the system, let $\boldsymbol{D}$ equal to $\boldsymbol{I}_2$. Therefore, the error vector e becomes equal to v. Referring to [13], if Equation (20) is proved, the system satisfies Lemma (a), as shown in Equation (21).

$$\boldsymbol{A}^{\boldsymbol{T}}\boldsymbol{P}+\boldsymbol{P}\boldsymbol{A}=-\boldsymbol{Q}<0 \tag{20}$$

Let $\boldsymbol{P}=\boldsymbol{I}_2$, then

$$\begin{aligned}\boldsymbol{A}^{\boldsymbol{T}}\boldsymbol{P}+\boldsymbol{P}\boldsymbol{A}&=\begin{bmatrix}-\frac{R_s}{L_d}&\omega_e\\-\omega_e&-\frac{R_s}{L_d}\end{bmatrix}+\begin{bmatrix}-\frac{R_s}{L_d}&-\omega_e\\\omega_e&-\frac{R_s}{L_d}\end{bmatrix}\\&=\begin{bmatrix}-\frac{2R_s}{L_d}&0\\0&-\frac{2R_s}{L_d}\end{bmatrix}=-\boldsymbol{Q}<0\end{aligned} \tag{21}$$

In order to satisfy Lemma (b), $\vec{w}$ of Equation (17) is separated into $\vec{w}_1\sim\vec{w}_4$, as shown in Equation (17). If Equations (23) $\sim$ (26) are proved, then Equation (22) is also proved, which means Lemma (b) is satisfied.

$$\eta(0,t_0)=\eta_1(0,t_1)+\eta_2(0,t_1)+\eta_3(0,t_1)+\eta_4(0,t_1)\geq-\kappa^2 \tag{22}$$

TABLE 2. Motor parameters for simulation.

SynRM Motor Parameters	Value	Unit
Motor inertia	0.005	kg-m^2
Damping Factor	0.0005	Nm-s/rad
Nominal Speed	1500	rpm
Rated Torque	32	Nm
Motor Poles	4	
d-axis Inductance L_d	201	mH
q-axis Inductance L_q	27	mH
Nominal Current	7.8	A(rms)

where

$$\eta_1(0,t_1)=\int_0^{t_1}\vec{e}^T\left(\frac{R_s}{L_d}-\frac{\hat{R}_s}{\hat{L}_d}\right)\begin{bmatrix}\hat{i}_\gamma\\\hat{i}_\delta\end{bmatrix}dt\geq-\kappa_1^2 \tag{23}$$

$$\eta_2(0,t_1)=\int_0^{t_1}\vec{e}^T\left(\frac{1}{\hat{L}_d}-\frac{1}{L_d}\right)\begin{bmatrix}u_\gamma\\u_\delta\end{bmatrix}dt\geq-\kappa_2^2 \tag{24}$$

$$\eta_3(0,t_1)=\int_0^{t_1}\vec{e}^T\left(\frac{\hat{\lambda}_a}{\hat{L}_d}\cos\varphi-\frac{\lambda_a}{L_d}\cos\varphi\right)\begin{bmatrix}\omega_e\\0\end{bmatrix}dt\geq-\kappa_3^2 \tag{25}$$

$$\eta_4(0,t_1)=\int_0^{t_1}\vec{e}^T\left(\frac{\hat{\lambda}_a}{\hat{L}_d}\sin\varphi-\frac{\lambda_a}{L_d}\sin\varphi\right)\begin{bmatrix}0\\\omega_e\end{bmatrix}dt\geq-\kappa_4^2 \tag{26}$$

Finally, the PI control law of parameter estimation can be designed, as shown in [13], [14], and the motor parameters can be calculated, as shown in Figure 10.

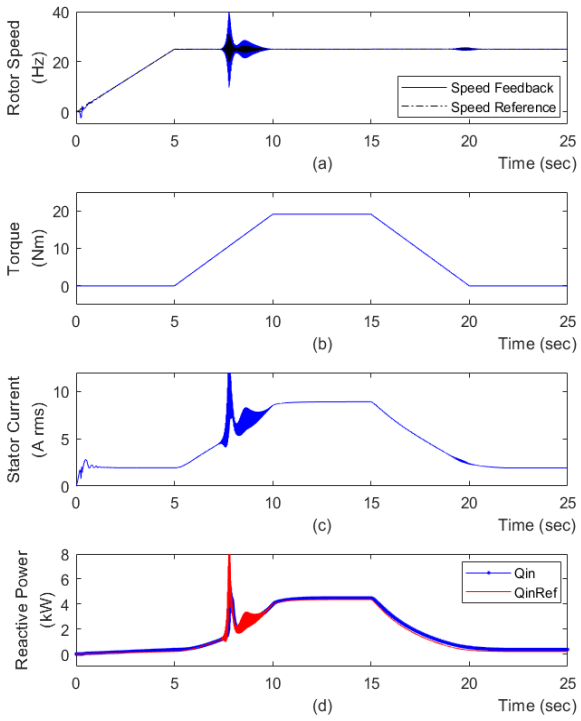

FIGURE 15. Ramp load test w/ stabilized loop and constant L_d (a) Rotor speed; (b) Load torque; (c) Stator current; (d) Reactive power.

The design procedure can be summarized in the following steps:

a. Use Equation (14) to implement the current observer.
b. Find the difference between the observer output current and the motor output current $\begin{bmatrix} e_\gamma & e_\delta \end{bmatrix}^T = \begin{bmatrix} (i_\gamma - \hat{i}_\gamma) & (i_\delta - \hat{i}_\delta) \end{bmatrix}^T$.
c. Use the adaptive law shown in Figure 10 to calculate $\hat{M}$, $\hat{N}$, $\hat{P}_d$ and $\hat{P}_q$.
d. Use $\hat{R}_s = \hat{M}/\hat{N}$, $\hat{L}_d = 1/\hat{N}$ and $\hat{\lambda}_a = \sqrt{\hat{P}_d^2 + \hat{P}_q^2}/\hat{N}$ to calculate estimated the parameters for the observer and scalar control loop.

IV. SIMULATION

In order to further verify the feasibility of the proposed adaptive scalar control of SynRMs, computer simulation is presented in this section using an ideal motor model. The nominal motor parameters are listed in Table 2, where L_d is a function of i_d, as shown in Figure 12. Note that L_d decreases when i_d increases with respect to load torque.

The simulation of the ideal motor model with constant parameters, as listed in Table 2, shows that, if there is no stabilized loop in the scalar control loop, the motor speed becomes unstable when the speed goes above 15Hz. However, if the stabilized loop is added into the scalar control, the speed will remain stable even when the load torque is applied to the motor, as shown in Figure 14(b).

If L_d is varied with respect to i_d, the stable system in Figure 14 would become unstable when the load torque increases above the 30% nominal torque, as shown in Figure 15. To avoid such unstable operation, an online estimation of L_d is used to calculate the reliable Q_{ref} of the MTPA loop, as shown in Figure 17. Once the L_d estimation is active with the gain of adaptive law, as listed in Table 3, the MTPA loop would generate the proper compensation voltage, and the speed would remain stable even if the load torque is exerted into the system, as shown in Figure 16.

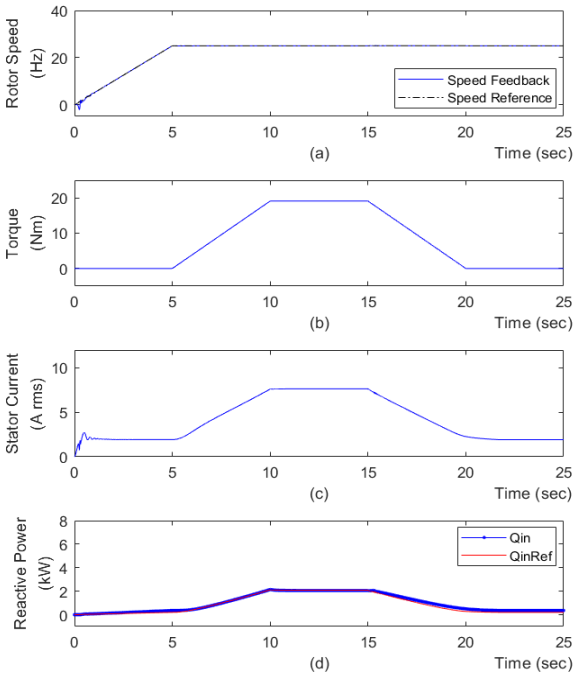

FIGURE 16. Ramp load test w/ stabilized loop and Estimated L_d (a) Rotor speed; (b) Load torque; (c) Stator current; (d) Reactive power.

TABLE 3. PI gain of parameter estimation.

PI Gain	Value	PI Gain	Value	PI Gain	Value
K_{pn}	0.001	K_{pfd}	0.001	K_{pfq}	0.001
K_{in}	0.1	K_{ifd}	0.05	K_{ifq}	0.0001

TABLE 4. Driver specifications.

Driver Spec.	Value
Rated Output Power	5.5kW
Rated Output Current	17A(RMS)
Rated Input Voltage	400-480V
Default PWMCarrier Frequency	8kHz

V. EXPERIMENTS

To verify the feasibility and performance of the proposed adaptive SynRM scalar control, experiments were carried out using a 5HP dynamometer, as shown in Figure 18. The control algorithm is implemented on the control board of a commercial motor drive CH2000, as made by Delta Electronics Incorporation. The SynRM motor used in the following experiments is shown in Figure 19, and the parameters are

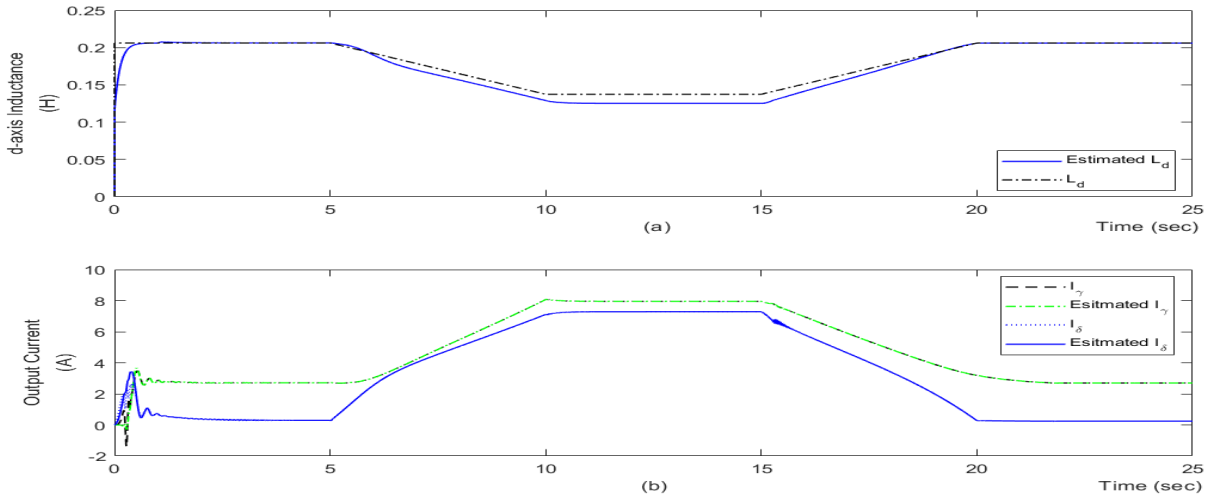

FIGURE 17. IPM parameters estimation in $\gamma\delta$-axis during ramp load test (a) L_d estimation and L_d reference value; (b) Estimated current and feedback current.

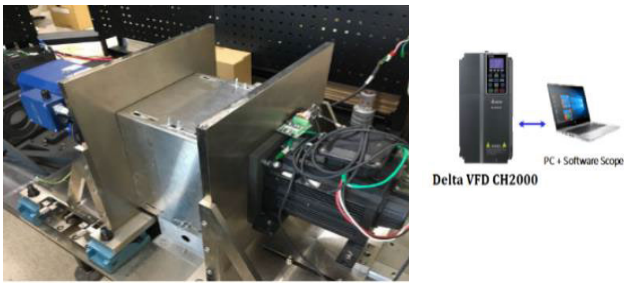

(a) Overall system of 5HP dynamometer (b) Delta VFD CH2000 Motor Drive

FIGURE 18. Test bench of 5HP Dynamometer.

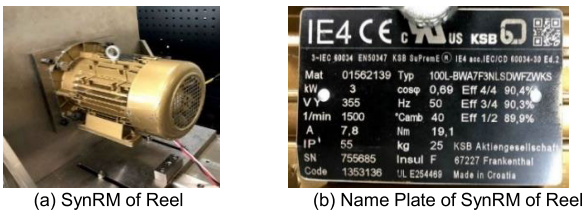

(a) SynRM of Reel (b) Name Plate of SynRM of Reel

FIGURE 19. Reel SynRM, for experiment.

listed in Table 5. The performances of the step load test and ramp load test are demonstrated to evaluate the performance of the proposed adaptive scalar control.

A 5.5kw driver, as shown in Figure 18(b), is chosen for this experiment, and the specifications of the driver are shown in Table 4.

A 3.0 kW SynRM motor, as shown in Figure 19(a), is chosen for this experiment. The specifications of the motor are shown in Table 5 and the nameplate information is shown in Figure 19(b).

As shown in Figure 20, if the SynRM scalar control uses a stabilized loop and MTPA loop without the L_d adaptation, the rotor speed becomes unstable when the load torque is increased to 60% of the rated torque, which is similar to simulation result shown in Figure 15. However, if the L_d

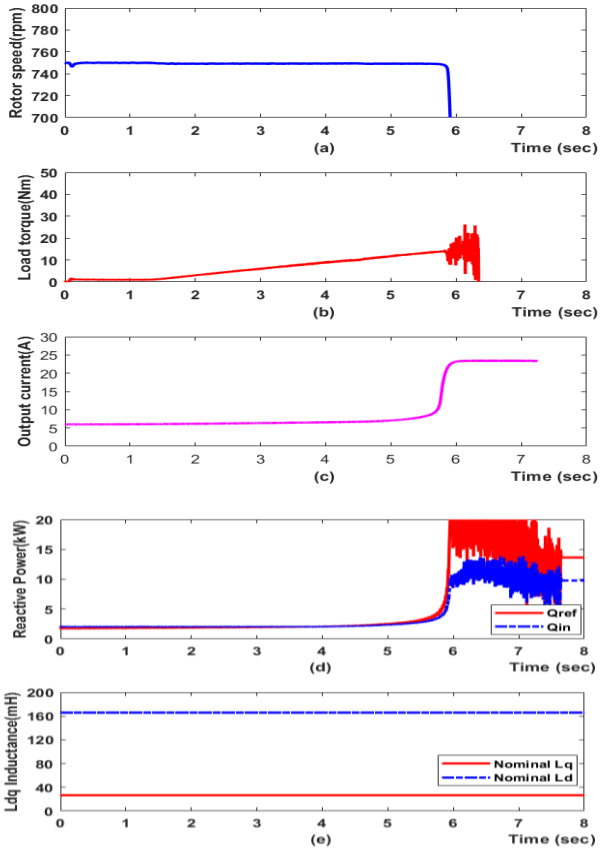

FIGURE 20. Ramp load test with constant dq-inductance (a) Rotor speed; (b) Load torque; (c) Stator current; (d) Reactive power; (e) Constant dq-axis inductance for reactive calculation.

adaptation works with a stabilized loop and MTPA loop during speed control, the rotor speed will remain stable even when a load torque as high as 200% of the nominal torque is exerted on the motor. As shown in Figure 21(e), L_d is estimated online to correctly calculate the reactive power,

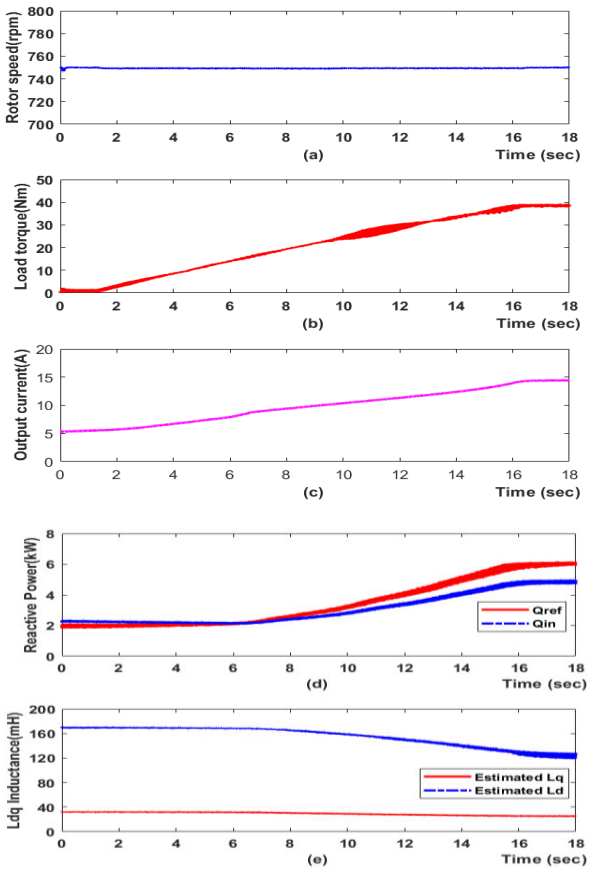

FIGURE 21. Ramp load test curve with estimated dq-inductance (a) Rotor speed; (b) Load torque; (c) Stator current; (d) Reactive power; (e) Estimated dq-axis inductance for reactive calculation.

TABLE 5. SynRM specifications.

SynRM Spec.	Value
Rated Power P_R	3.0 kW
Rated Voltage V_{ac}	380 V (rms)
Rated Current I_R	7.8A (rms)
Rated Torque T_R	19.1 Nm
Rated Speed ω_R	1500 rpm
Pole Number N_P	4
d-axis Inductance L_d	115 mH

which causes the MTPA loop function properly and maintains the optimal output current. Verification of the output current is shown in Figure 21(c), where the output current is 14.9A, about 200% nominal current. When the load torque reaches the 200% nominal torque, it proves that the MTPA loop functions properly with the aid of the online adoption of L_d.

Furthermore, if 150% rated torque step load is exerted, Figure 22 shows that the ability of the SynRM scalar control to reject disturbance is quite excellent at speeds ranging from 1/10 rated speed to 100% rated speed. In addition, even in the low very low speed region and flux-weakening region, speed control can keep stable with 100% step load

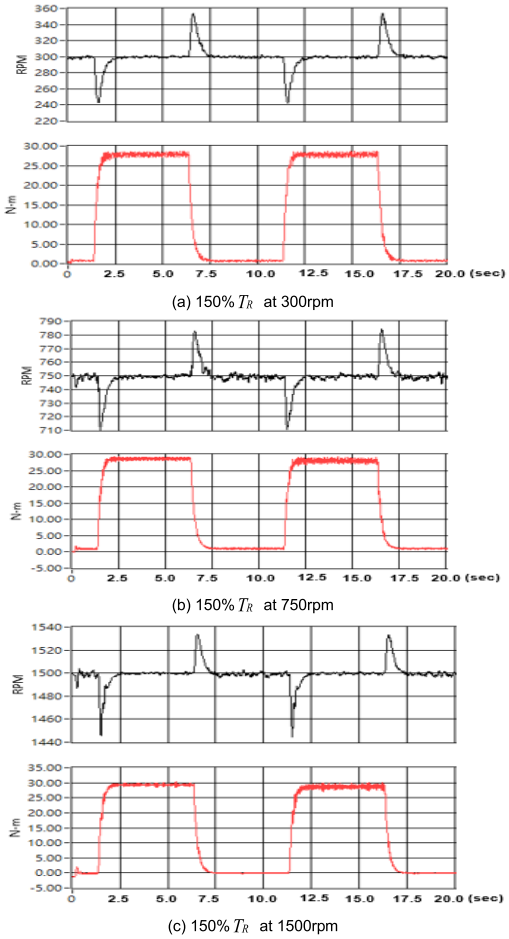

FIGURE 22. 150% step load test at 10%,50%,100% rated speed.

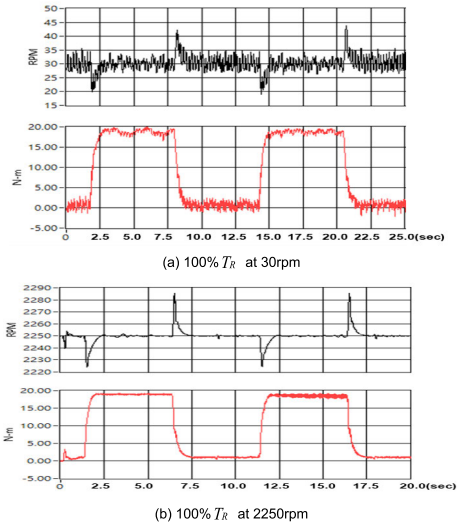

FIGURE 23. 100% step load test at 5% and 150% rated speed.

as shown in Figure 23. All the experimental data show that the proposed method features high stability and efficiency, which is almost the same as the FOC current vector control presented in [5], making it qualified for industrial applications.

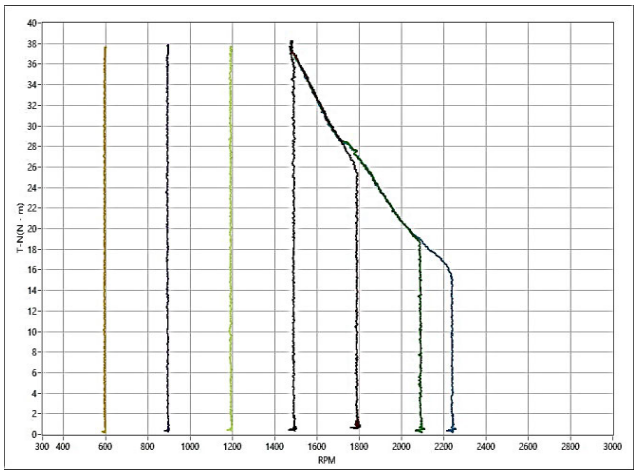

(a) TN curve at the high speed region of FOC control

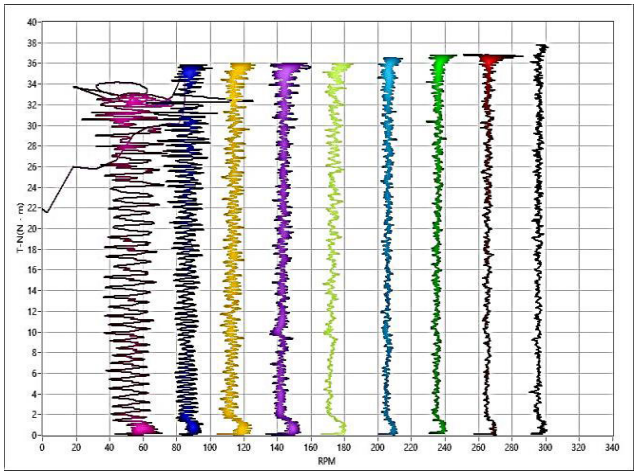

(b) TN curve at the low speed region of FOC control

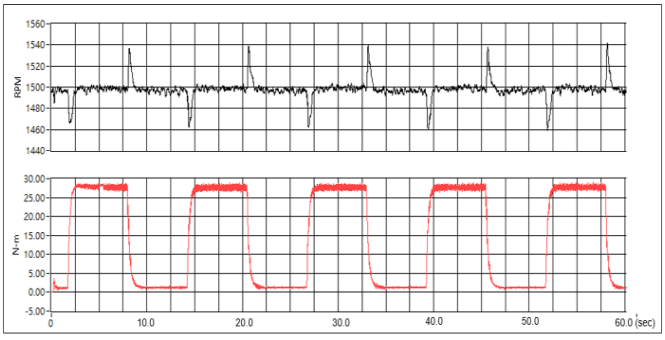

(c)150% step load test of FOC control

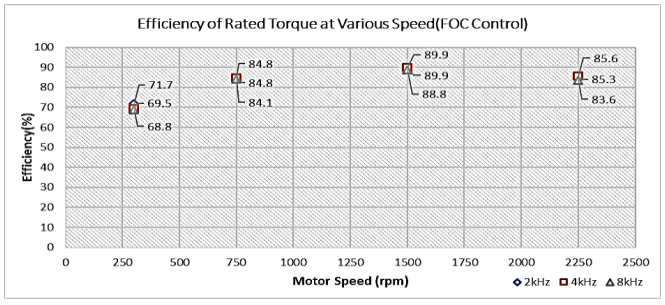

(d)Efficiency of FOC control w/ different PWM switching frequency

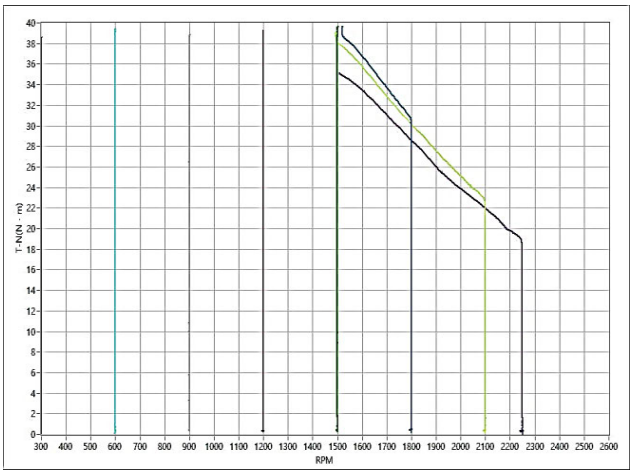

(e) TN curve at the high speed region of scalar control

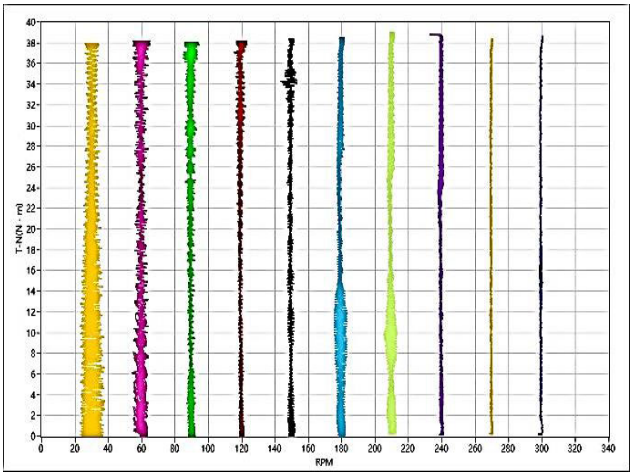

(f) TN curve at the low speed region of scalar control

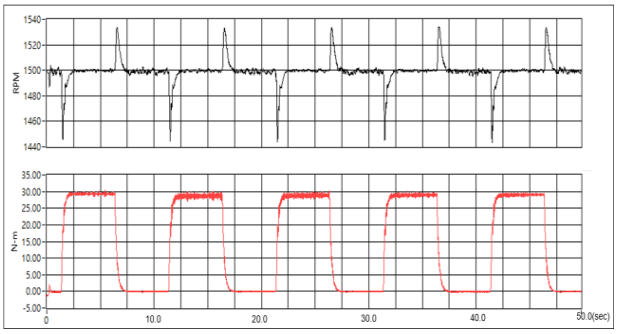

(g)150% step load test of scalar control

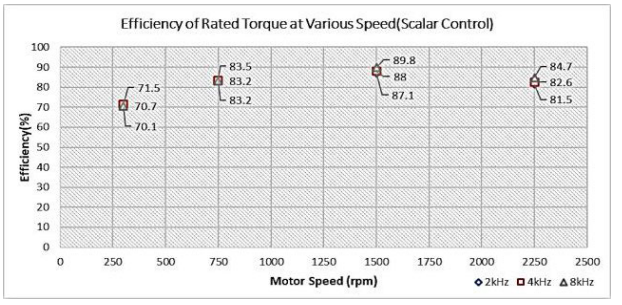

(h) Efficiency of scalar control w/ different PWM switching frequency

FIGURE 24. **100% step load test at 5% and 150% rated speed.**

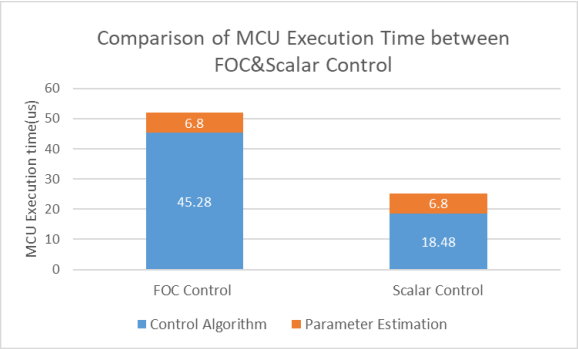

FIGURE 25. 100% step load test at 5% and 150% rated speed.

TABLE 6. SynRM scalar control performance comparison.

	Reference [8] with efficiency optimization+ Stability prediction &protection		Proposed paper with stable loop+MTPA+ voltage compensation &parameter estimation	
Speed(Hz)	Maximum Load torque	Slew Rate	Maximum Load torque	Slew Rate
75Hz(150%)	-	-	100	0.5
50Hz(100%)	100%	0	150	0
37.5Hz(75%)	100%	0	150	0
25Hz(50%)	100%	0	150	0
12.5Hz(25%)	85-100%	5s	150	0
5Hz(10%)	-	-	150	0
1Hz(1%)	-	-	100	0.5

In order to verify the performance of the scalar control, Figure 24 shows the comprehensive comparison of the performance, such as TN curves, step load test, and efficiency performance test, between scalar control and FOC, which is commonly used in SynRM sensorless control due to the fast torque response.

The efficiency is also measured for different PWM switching frequency. As illustrated shown in Figure 24(d) and Figure24 (h), the efficiency is close to nominal value in high speed region but getting lower in low speed due to higher no low current for the sake of stability.

A comparison report of the computation resource shown in Figure 25 indicates that computation resource requirement of Scalar Control is much fewer than that of FOC Control. If online parameter estimation function is enabled for scalar control, the total execution time for main algorithm would increase 6.8μs (i.e. from 18.48μs to 25.28μs). Although online parameter estimation is about 27% of total execution time in scalar control, it however, upgrades the performance of scalar control a lot as illustrated in Figure 20 and Figure 21. As for the FOC control, the total execution time is 45.28us with online parameter estimation. If online parameter estimation function is enabled for the FOC, the execution time of the FOC is 206% execution time of the scalar control. The comparison in Figure 25 shows the computational efficiency of the scalar control is superior to that of FOC.

The above comparison shows that the proposed scalar control could has performance as good as FOC control. The overall stability performance listed in Table 6 also shows that compared to the performance of [8], proposed method can even keep stable with 150% step load torque and also can operate in 1% rated speed and 150% rated speed, which indicates that the proposed scalar control is qualified for most of the speed control applications.

VI. CONCLUSION

The contributions of this paper are summed up as follows:

1) Based on the steady state model, voltage command for the scalar control of SynRMs is proposed.
2) By means of MTPA analysis, the voltage compensation loop is proposed, and is verified by simulation and experimentation to be stable and highly efficient.
3) Online estimation of the motor parameters, especially for L_d, is proposed to make the MTPA loop function properly with precise inductance, which makes the proposed scalar control robust and reliable.
4) Comprehensive experiments and comparison show that the proposed adaptive scalar control features both stability and improved efficiency even compared to sensorless FOC control.

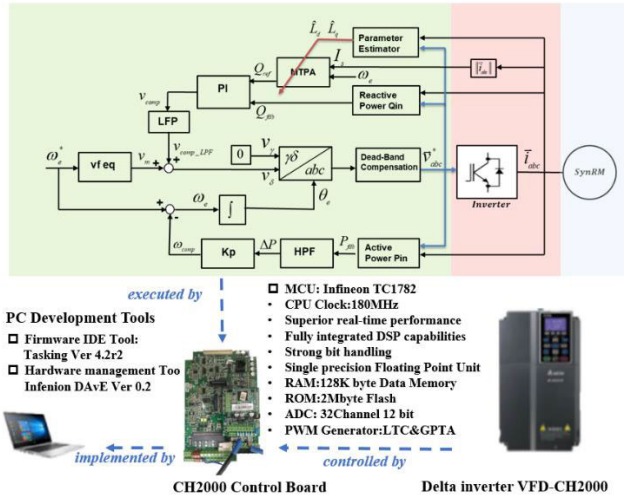

FIGURE 26. Development Environment of the control system and key specification of the TC1782 Tricore DSP.

APPENDIX

The SynRM scalar control system of SynRM proposed in this paper is implemented on control board of a VFD-CH2000 drive. The processing unit of the control board is Infenion TC1782 Tricore DSP with high performance signal processing capability and a PWM generator for motor control. The key specifications of the TC1782 are listed in Figure 26. The control system is developed by Eclipse Tasking IDE v4.2r2 which can help users to develop high performance control and signal processing algorithms based on the DSP instruction sets.

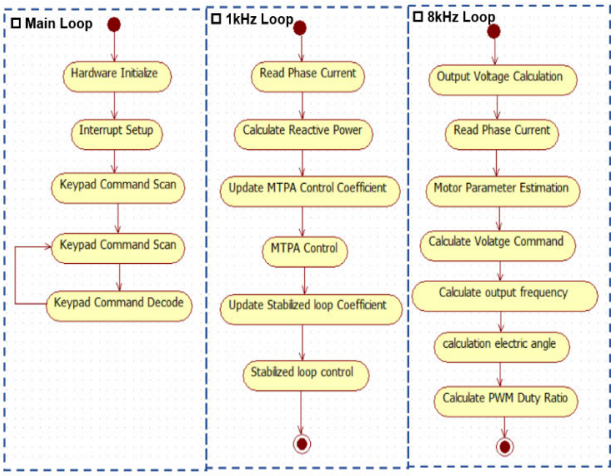

FIGURE 27. Flow chart of scalar control of SynRMs in different time loop.

The scalar control system is implemented in the main loop and two timer interrupt loops as shown in Figure 27. The main, 1kHz and 8kHz timer interrupt loop are executed in TC1782 to implemented the coefficient calculation, MTPA loop, stabilized loop and motor parameter estimation. The 8k interrupt has highest priority, and 1k Hz also has higher priority than main loop to execute MTAP and stabilized loop.

REFERENCES

[1] A. T. D. Almeida, F. J. T. E. Ferreira, and G. Baoming, "Beyond induction motors—Technology trends to move up efficiency," *IEEE Trans. Ind. Appl.*, vol. 50, no. 3, pp. 2103–2114, May 2014, doi: 10.1109/TIA.2013.2288425.

[2] S. Piriienko, U. Ammann, M. Neuburger, F. Bertele, T. Roser, A. Balakhontsev, N. Neuberger, and P.-W. Cheng, "Influence of the control strategy on the efficiency of SynRM based small-scale wind generators," in *Proc. IEEE Int. Conf. Ind. Technol. (ICIT)*, Melbourne, VIC, Australia, Feb. 2019, pp. 280–285, doi: 10.1109/ICIT.2019.8755122.

[3] S. Yamamoto, J. B. Adawey, and T. Ara, "Maximum efficiency drives of synchronous reluctance motors by a novel loss minimization controller considering cross-magnetic saturation," in *Proc. IEEE Energy Convers. Congr. Expo.*, San Jose, CA, USA, Sep. 2009, pp. 288–293, doi: 10.1109/ECCE.2009.5316379.

[4] M. N. Ibrahim, P. Sergeant, and E. M. Rashad, "Synchronous reluctance motor performance based on different electrical steel grades," *IEEE Trans. Magn.*, vol. 51, no. 11, pp. 1–4, Nov. 2015, doi: 10.1109/TMAG.2015.2441772.

[5] P. R. Ghosh, A. Das, and G. Bhuvaneswari, "Performance comparison of different vector control approaches for a synchronous reluctance motor drive," in *Proc. 6th Int. Conf. Comput. Appl. Electr. Eng.-Recent Adv. (CERA)*, Roorkee, India, Oct. 2017, pp. 320–325, doi: 10.1109/CERA.2017.8343348.

[6] S. M. Ferdous, P. Garcia, M. A. M. Oninda, and M. A. Hoque, "MTPA and field weakening control of synchronous reluctance motor," in *Proc. 9th Int. Conf. Electr. Comput. Eng. (ICECE)*, Dhaka, Bangladesh, Dec. 2016, pp. 598–601, doi: 10.1109/ICECE.2016.7853991.

[7] P. D. C. Perera, F. Blaabjerg, J. K. Pedersen, and P. Thogersen, "A sensorless, stable v/f control method for permanent-magnet synchronous motor drives," *IEEE Trans. Ind. Appl.*, vol. 39, no. 3, pp. 783–791, May 2003, doi: 10.1109/TIA.2003.810624.

[8] G. Jalali, S. Ahmed, H. Kim, and Z. Pan, "Instability detection and protection scheme for efficiency optimized v/f driven synchronous reluctance motors (SynRM)," in *Proc. IEEE Energy Convers. Congr. Expo. (ECCE)*, Milwaukee, WI, USA, Sep. 2016, pp. 1–6, doi: 10.1109/ECCE.2016.7855206.

[9] M. Cacciato, A. Consoli, G. Scarcella, and G. Scelba, "A novel efficiency optimization scalar control technique for industrial IPMSM drives," in *Proc. IEEE Int. Symp. Ind. Electron.*, Bari, Italy, Jul. 2010, pp. 1181–1186, doi: 10.1109/ISIE.2010.5636642.

[10] P. Niazi, H. A. Toliyat, and A. Goodarzi, "Robust maximum torque per ampere (MTPA) control of PM-assisted SynRM for traction applications," *IEEE Trans. Veh. Technol.*, vol. 56, no. 4, pp. 1538–1545, Jul. 2007, doi: 10.1109/TVT.2007.896974.

[11] Z. Tang, X. Li, S. Dusmez, and B. Akin, "A new V/f-based sensorless MTPA control for IPMSM drives," *IEEE Trans. Power Electron.*, vol. 31, no. 6, pp. 4400–4415, Jun. 2016, doi: 10.1109/TPEL.2015.2470177.

[12] S.-M. Sue, T.-W. Hung, J.-H. Liaw, Y.-F. Li, and C.-Y. Sun, "A new MTPA control strategy for sensorless V/f controlled PMSM drives," in *Proc. 6th IEEE Conf. Ind. Electron. Appl.*, Beijing, China, Jun. 2011, pp. 1840–1844, doi: 10.1109/ICIEA.2011.5975891.

[13] Y. Chen, F. Zhou, X. Liu, and E. Hu, "Online adaptive parameter identification of PMSM based on the dead-time compensation," *Int. J. Electron.*, vol. 102, no. 7, pp. 1132–1150, Jul. 2015.

[14] L.-J. Cheng and M.-C. Tsai, "Enhanced model predictive direct torque control applied to IPM motor with online parameter adaptation," *IEEE Access*, vol. 8, pp. 42185–42199, 2020, doi: 10.1109/ACCESS.2020.2977057.

[15] Y. Inoue, Y. Kawaguchi, S. Morimoto, and M. Sanada, "Performance improvement of sensorless IPMSM drives in a low-speed region using online parameter identification," *IEEE Trans. Ind. Appl.*, vol. 47, no. 2, pp. 798–804, Mar. 2011.

[16] Y. Shi, K. Sun, L. Huang, and Y. Li, "Online identification of permanent magnet flux based on extended Kalman filter for IPMSM drive with position sensorless control," *IEEE Trans. Ind. Electron.*, vol. 59, no. 11, pp. 4169–4178, Nov. 2012.

[17] K. Liu, Q. Zhang, Z.-Q. Zhu, J. Zhang, A.-W. Shen, and P. Stewart, "Comparison of two novel MRAS based strategies for identifying parameters in permanent magnet synchronous motors," *Int. J. Autom. Comput.*, vol. 7, no. 4, pp. 516–524, Nov. 2010.

[18] S. J. Underwood and I. Husain, "Online parameter estimation and adaptive control of permanent-magnet synchronous machines," *IEEE Trans. Ind. Electron.*, vol. 57, no. 7, pp. 2435–2443, Jul. 2010.

LON-JAY CHENG was born in Ping-Tung, Taiwan, in 1977. He received the B.S. degree in mechanical engineering from National Taiwan University, in 1999, and the M.S. degree in mechanical engineering from National Chiao Tung University, in 2001. He is currently pursuing the Ph.D. degree in mechanical engineering with National Cheng Kung University, Tainan, Taiwan.

From 2001 to 2005, he was a Research Assistant with NCSIST, Taoyuan, Taiwan. Since 2007, he has been a Firmware Engineer with Delta Electronics INC., Tainan. He is also an Assistant Manager of IABG of Delta Electronics Inc. He holds eight patents. His research interests include sensorless FOC&DTC control of IM/PM/SynRM AC motor, and adaptive control and robust control in motor control application.

MI-CHING TSAI (Fellow, IEEE) received the Ph.D. degree in engineering science from the University of Oxford, Oxford, U.K., in 1990.

He is currently a Chair Professor with the Department of Mechanical Engineering, National Cheng Kung University, Taiwan. He authored or coauthored more than 127 journal articles. He holds more than 122 patents. His research interests include robust control, servo control, motor design, and applications of advanced control technologies using DSPs.

Dr. Tsai is a Fellow of the Institution of Engineering and Technology, U.K. From 2003 to 2007, he was an Associate Editor of the IEEE/ASME TRANSACTIONS ON MECHATRONICS. From 2016 to 2017, he was the Deputy Minister of Ministry of Science and Technology, Taiwan.